Phase transformation pathways of ultrafast-laser-irradiated Ln$_2$O$_3$ (Ln = Er–Lu)

Dylan R. Rittman,[1] Cameron L. Tracy,[1] Chien-Hung Chen,[1] Jonathan M. Solomon,[2] Mark Asta,[2] Wendy L. Mao,[1,3] Steven M. Yalisove,[4] and Rodney C. Ewing[1]

[1]*Department of Geological Sciences, Stanford University, Stanford, California 94305, USA*
[2]*Department of Materials Science and Engineering, University of California, Berkeley, California 94720, USA*
[3]*Stanford Institute for Materials and Energy Sciences, SLAC National Accelerator Laboratory, Menlo Park, California 94025, USA*
[4]*Department of Materials Science and Engineering, University of Michigan, Ann Arbor, Michigan 48109, USA*

Ultrafast laser irradiation causes intense electronic excitations in materials, leading to transient high temperatures and pressures. Here, we show that ultrafast laser irradiation drives an irreversible cubic-to-monoclinic phase transformation in Ln$_2$O$_3$ (Ln = Er–Lu), and explore the mechanism by which the phase transformation occurs. A combination of grazing incidence x-ray diffraction and transmission electron microscopy are used to determine the magnitude and depth-dependence of the phase transformation, respectively. Although all compositions undergo the same transformation, their transformation mechanisms differ. The transformation is pressure-driven for Ln = Tm–Lu, consistent with the material's phase behavior under equilibrium conditions. However, the transformation is thermally driven for Ln = Er, revealing that the nonequilibrium conditions of ultrafast laser irradiation can lead to novel transformation pathways. *Ab initio* molecular-dynamics simulations are used to examine the atomic-scale effects of electronic excitation, showing the production of oxygen Frenkel pairs and the migration of interstitial oxygen to tetrahedrally coordinated constitutional vacancy sites, the first step in a defect-driven phase transformation.

I. INTRODUCTION

Irradiation by ultrafast lasers induces highly nonequilibrium conditions in materials over short time scales, causing damage in the near-surface region [1–3]. Thus, ultrafast lasers are important as an advanced materials processing tool, with applications ranging from the fabrication of semiconductor nanostructures [4,5] to low collateral damage drilling of structural materials [6,7]. Additionally, ultrafast lasers can induce phase transformations to both high-temperature [8] and high-pressure [9–11] polymorphs, as well as novel phases not achieved through conventional processing methods [12,13].

Ultrafast laser irradiation causes a multistage damage process in ionic-covalent materials. Defining this process is important in order to obtain a mechanistic understanding of ultrafast laser-induced material modifications. The process is initiated by electronic excitation in the near surface (∼100-nm depth) over the course of the ∼100-fs pulse duration [2]. This excitation of electrons from the valance band to the conduction band (bonding to antibonding orbitals) alters the interatomic potentials between atoms [14]. This change in bonding persists for subpicosecond time scales, leading to phenomena such as nonthermal melting [14,15] and point-defect generation [4,16]. Electron-phonon coupling occurs as electrons recombine from ∼1−10 ps, causing local heating that can induce melting [1,2]. Expansion and ablation of the laser-excited near-surface launches a strain wave deeper into the material, from ∼10−100 ps, that can cause plastic deformation and transient high-pressure states [1]. Finally, thermal diffusion returns the material to ambient conditions over nanosecond time scales [2]. Thus, there are transient electronic, thermal, and pressure damage mechanisms, which can all cause irreversible material modifications.

Here, we report the responses of Ln$_2$O$_3$ (Ln = Er–Lu) materials to ultrafast laser irradiation, which is shown to induce a cubic-to-monoclinic (C→B) phase transformation. Recently, much work has gone into trying to understand ultrafast laser-driven phase transformations [8–13]. Gaining a mechanistic understanding of how and why these transformations occur is an important step in being able to more effectively use ultrafast lasers for materials processing. The chemical similarity of the lanthanides, and their gradual contraction across the series, makes their oxides a useful system for investigating trends in phase behavior.

In order to analyze the phase behavior of Ln$_2$O$_3$ under the highly nonequilibrium conditions induced by ultrafast laser irradiation, it is first necessary to understand their equilibrium phase behavior under high-temperature and high-pressure conditions. A similar trend is observed in both the high-temperature and high-pressure phase diagrams as a function of lanthanide species (Fig. 1): a change in phase stability from trigonal → monoclinic → cubic ($A → B → C$) as lanthanide atomic number increases. This progression of stable phases is caused by lanthanide contraction—the monotonic decrease of lanthanide ionic radius as atomic number increases due to poor screening of nuclear charge by f electrons. The A-type phase is energetically favored for larger lanthanides due to its sevenfold cation coordination, while C type is favored for smaller lanthanides due to its sixfold cation coordination. The B-type phase, a mixture of six- and sevenfold cation coordination, is favored for intermediate-sized lanthanides [29].
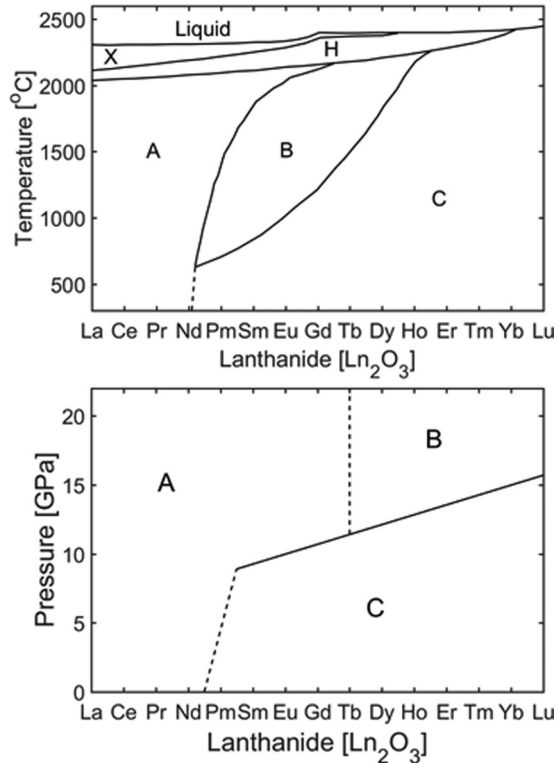
FIG. 1. High-temperature (top) and high-pressure (bottom) phase diagrams of Ln_2O_3 materials. Phases are: A type (trigonal P-$3m1$), B type (monoclinic $C2/m$), C type (face-centered cubic Ia-3), H type (hexagonal $P6_3/mmc$), and X type (body-centered cubic Im-$3m$). Dashed lines represent approximate phase boundaries. The high-temperature phase diagram is adapted from Ref. [17]. The high-pressure phase diagram is constructed using data from Refs. [18–28].

The compounds investigated here have similar equilibrium phase behavior: all are C type at ambient conditions, transform to B type at high pressure, and do not transform to B type at high temperature. Notably, throughout the Ln_2O_3 series, the B-type structure is retained upon returning to ambient conditions following its synthesis at high temperature or high pressure due to the reconstructive nature [30] of the largely irreversible phase transformation.

II. METHODS

A. Experimental

Powders of Ln_2O_3 (Ln = Er–Lu) were pressed into pellets of $\sim$1-cm diameter, and sintered at high temperature in stagnant air at ambient pressure. Samples were heated at a rate of 1 $^\circ$C min^{-1} to a temperature of 1200 $^\circ$C, held for 50 h, then cooled to ambient temperature at a rate of 1 $^\circ$C min^{-1}. This produced pellets of $\sim$90% theoretical density. X-ray diffraction of the samples following preparation confirmed that the all compounds were purely C type.

Samples were then irradiated by a Clark MXR Ti:sapphire laser with a wavelength of 780 nm, maximum pulse energy of 800 μJ, pulse duration of 150 fs, and maximum repetition rate of 1 kHz. The laser was focused through a 20-cm focal length lens to a $1/e^2$ focal diameter of $\sim$45 μm, as measured

by a DataRay WinCamD beam profiler. All irradiations were at a peak fluence of 40 J cm^{-2}, which produced damage spots of $\sim$70 μm diameter. The full surface of each sample was irradiated by moving the sample in a raster pattern—a 35-μm step size (half of the damage diameter) was taken between laser exposures in order to create a more uniform fluence profile across the entirety of the sample surface.

Irradiated samples were analyzed using grazing incidence x-ray diffraction (GIXRD) and transmission electron microscopy (TEM). GIXRD was conducted at beamline 11–3 of the Stanford Synchrotron Light Source (SSRL), SLAC National Accelerator Laboratory with $\lambda = 0.9762$ Å. LaB$_6$ was used as a calibrant. Data were collected for 30 s at incidence angles of 3° and 4° for each sample. Radial integration of raw data into diffraction patters was performed using DIOPTAS [31]. MAUD was used for Rietveld refinement of the integrated patterns [32].

TEM was used to conduct bright-field imaging and selected area electron diffraction (SAED) both at the surface and deeper into the bulk ($\sim$215 nm) of Er$_2$O$_3$ and Lu$_2$O$_3$. Cross-sectional TEM samples were prepared through mechanical polishing using sequential lapping films of decreasing roughness, from 30 μm down to 1 μm. Ion milling was performed using Ar$^+$ ions of 3$-$5-keV energy at an angle of 87° from the surface normal to achieve electron transparency. TEM studies were performed using an FEI Tecnai Transmission Electron Microscope at the Stanford Nano Shared Facilities (SNSF) operated at 200 kV. A double tilt holder with a $\pm 30^\circ$ tilting limit was used to tilt specific grains to the zone axis. Bright-field imaging, with 2.5-Å point-to-point resolution, was used to analyze microstructure. SAED was employed to determine the crystal structure, which was analyzed using CRYSTALMAKER.

B. Computational

Ab initio molecular-dynamics simulations were undertaken to provide insights into the effects of electronic excitation induced by the laser pulse on atomic structure. Such simulations have been used extensively in studies of the structure and dynamics of materials in response to ultrafast laser pulses [33–40]. It is emphasized that the purpose of employing such simulations in the present work was not to replicate experimental conditions. Rather, the aim was a more modest one of probing the effects of electronic excitation on the structure and dynamics of Ln_2O_3 compounds.

The simulations were performed within the Perdew-Burke-Ernzerhof generalized-gradient approximation [41] to density-functional theory, using the projector-augmented-wave method [42,43] and a plane-wave basis set, as implemented in the Vienna *Ab Initio* Simulation Package [44,45]. Ln = Gd and Lu were considered since the occupied $4f$ electrons in these Ln_2O_3 compounds are furthest from the valence-band maximum [46]. Thus, they can be reasonably approximated as core-electron states in the simulations. The simulations made use of a Mermin functional with an electron temperature set to that of a characteristic experimental band gap for the rare-earth sesquioxides ($\sim$5.2 eV, 60 000 K), and the ionic positions were evolved by integrating Newton's equations of motion using the interatomic forces derived from this functional.

Following equilibration of the system at 300 K, the electronic temperature was raised to 60 000 K ($\sim$5.2 eV) for a period of 150 fs. After each of these simulations, the final configuration was used as an input to an energy-minimization calculation in which the ions were relaxed to nearest local minimum-energy positions using a conjugate-gradient algorithm, with energy and forces corresponding to the zero-temperature energy surface, to analyze whether Ln or O ions had moved out of their ground-state energy basins to new ones associated with interstitial defect sites. Relaxation of ionic positions were carried out until the total energy change between ionic steps was within 10^{-3} eV, such that the average magnitude of the residual forces on the ions was below approximately $10 \, \mathrm{meV \, \mathring{A}^{-1}}$. 114 such simulations and relaxations were undertaken for both Gd_2O_3 and Lu_2O_3, and the final relaxed configurations were analyzed to determine the number and position of point defects formed. Further details of the simulations can be found in the Supplemental Material [47].

III. RESULTS AND DISCUSSION

A. Experimental

GIXRD patterns of Ln_2O_3 following ultrafast laser irradiation are shown in Fig. 2(a). All compounds underwent a C→B phase transformation. Equilibrium phase behavior of these materials would suggest a pressure-based transformation mechanism. Ultrafast laser irradiation at similar intensities to those used here ($\sim10^{14}$ W cm^{-2}) have been shown to generate shock waves well in excess of the C→B transformation pressure [48–51]. Notably, these shock waves have extremely short durations ($\sim$10 ps) [48,51], and decay rapidly upon traversing the material—with $1/e$ pressure losses on the order of $\sim100-150$-nm depths [49]. The possible duration of a pressure-induced phase transformation would be limited by the duration of the shock wave, suggesting that a pressure-induced phase transformation would require extremely fast kinetics ($\sim$10 ps), even though the C→B phase transformation in Ln_2O_3 is reconstructive.

The B-type phase fraction of all compounds was determined using Rietveld refinement. Results of phase-fraction refinements are shown in Fig. 2(b). Analysis was performed for GIXRD data collected at both 3° and 4° incident angles. Linear interpolation was the used to estimate the phase fraction for an x-ray penetration depth of 200 nm, which corrected for the changing x-ray penetration depth with sample composition. Relative phase fractions between the different compounds were not found to be sensitive to the choice of x-ray penetration depth, showing that this analysis is robust.

The amount of B-type phase produced was found to decrease with increasing lanthanide mass. However, there is a markedly greater B-type phase fraction in Ln = Er as compared with Ln = Tm–Lu. This discrepancy suggests that there may be a different mechanism driving the phase transformation in Ln = Er vs Ln = Tm–Lu. Again, based on the equilibrium phase behavior of these materials, a pressure-induced phase transformation would be expected for all of the compositions. However, Er_2O_3 exists just beyond the stability field of the B-type phase at equilibrium high-temperature conditions (see Fig. 1). Thus, it is possible that the rapid heating and quenching
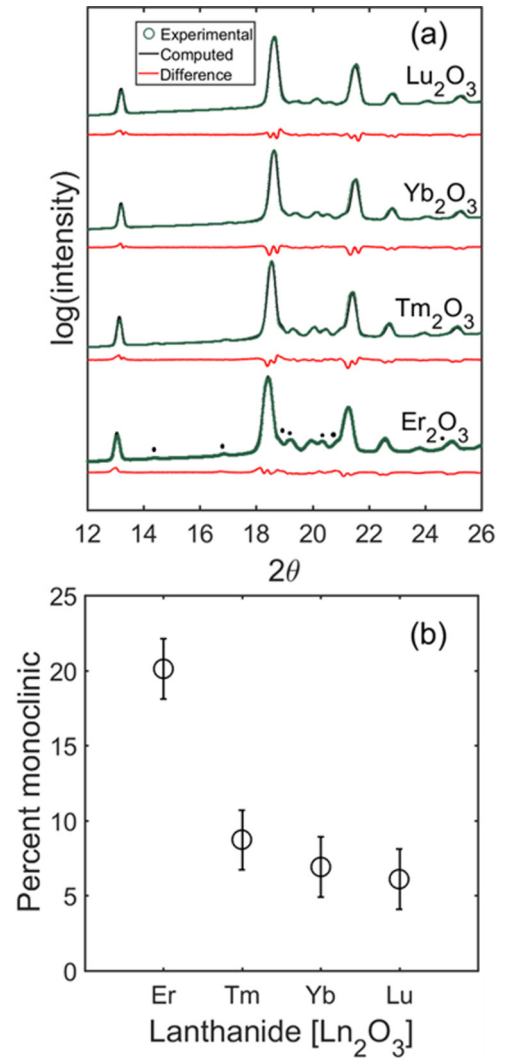

FIG. 2. (a) GIXRD patterns of Ln_2O_3 (Ln = Er–Lu) measured at a 3° incident angle with $\lambda = 0.9762 \, \mathring{A}$. Experimental data (green circles) are overlaid on computed diffraction patterns from Rietveld refinement (black lines). Red lines represent the difference between the computed and experimental diffraction patterns. Black dots above the Er_2O_3 diffraction pattern identify maxima from the B-type phase. The y axis is logarithmic to better display the low-intensity monoclinic signal. (b) Results of phase-fraction analysis from Rietveld refinement showing the percent of monoclinic phase for an x-ray penetration depth of 200 nm.

rates associated with ultrafast laser irradiation permit the formation of the B-type phase through a high-temperature pathway.

Characterizing the depth dependence of the phase transformation can help elucidate the mechanism driving the phase transformation. After irradiation-induced heating and subsequent thermal diffusion, a residual "heat-affected zone" exists in the near-surface of the material. Experiments have shown that at fluences well above the threshold for material ablation, such as those used here, the heat-affected zone following ultrafast laser irradiation is very shallow [6,52,53]. Cross-sectional high-resolution TEM has shown that this zone can be as shallow as a few tens of nm in ionic-covalent materials
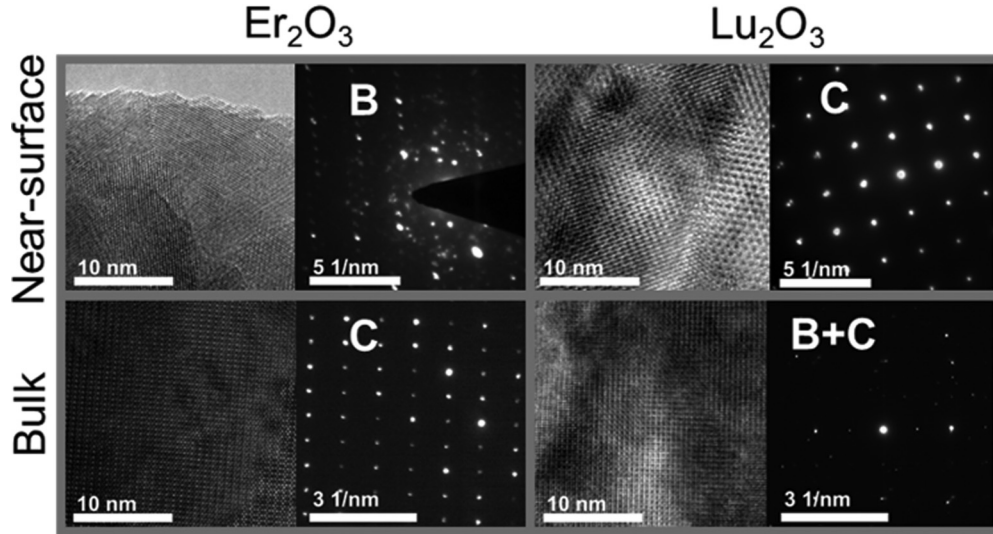
FIG. 3. Cross-sectional TEM of irradiated Er_2O_3 and Lu_2O_3. High-resolution bright-field images and SAED patterns are shown for the near-surface (0-nm depth) and bulk (200-nm depth for Er_2O_3, 230-nm depth for Lu_2O_3). Observed phases are indicated in the SAED patterns.

[30]. Damage from the high-pressure strain wave, driven by the expansion of the laser-excited near-surface, extends deeper into the bulk [6,54]. Hydrodynamic simulations have also explored this phenomenon [51], with the simulations agreeing well with experiments.

Cross-sectional TEM of Er_2O_3 and Lu_2O_3, the compositions with the lightest and heaviest lanthanide elements among those studied, are shown in Fig. 3. Bright-field images and SAED patterns from both the near-surface (0-nm depth) and deeper into the bulk of the pellets (~215-nm depth) are included. A mechanistic understanding of the phase transformation can be achieved by correlating the depth of the transformation with the heat-affected zone.

SAED characterization of the bulk of the Lu_2O_3 sample shows a mixture of the B- and C-type phases, consistent with a pressure-induced phase transformation based on the depth to which strain waves typically penetrate. This transformation mechanism is representative of the material's equilibrium phase behavior, which is noteworthy considering the highly nonequilibrium nature of ultrafast laser irradiation. Two-phase coexistence is expected for phase transformations driven by shock waves from ultrafast lasers since the short (~10 ps) shock duration does not allow for extensive growth of the new phase [11]. The thermally affected material near the surface retained the original C-type phase.

Conversely, SAED of Er_2O_3 shows predominantly B-type phase in the near-surface and only C-type phase in the bulk. This more complete transformation is consistent with a thermal process [30] due to the much longer time scale of thermal diffusion compared with shock-wave propagation. Furthermore, high-resolution bright-field images show a reduction in grain size in the near-surface of Er_2O_3—multiple grains are observed in the near-surface image while a single grain is observed in the bulk. This reduction in grain size is consistent with thermally induced recrystallization in the heat-affected near-surface. Thus, the transient extreme conditions of ultrafast laser irradiation facilitated a nonequilibrium thermal phase-transformation pathway in Er_2O_3.

To date, little is understood about the processes governing phase behavior under highly nonequilibrium conditions. The difference in the behaviors of Er_2O_3 and Lu_2O_3 allows important observations to be made, such as how the susceptibility of Er_2O_3 to a thermally driven transformation corresponds to an extension of the B-type phase-stability field in the equilibrium high-temperature phase diagram (Fig. 1). It also establishes that identical irradiations of physically and chemically similar Ln_2O_3 compounds can lead to different phase-transformation pathways, emphasizing how subtle changes can greatly affect dynamical material behavior.

B. Computational

Isolating the effects of electronic excitation is also important to assessing the overall process of ultrafast laser irradiation. Even low-energy irradiation, well below the single-shot ablation threshold, is believed to generate point defects [4,16]. Repeated irradiation below the damage threshold can lead to defect accumulation, causing defect-driven phase transformations [8]. These electronic excitation-induced, defect-driven phase transformations have also been observed in materials irradiated with swift heavy ions (SHIs) [30,55], which deposit their energy primarily through intense electronic excitations and have a similar damage process to ultrafast lasers [1,8]. Notably, SHIs have induced C→B transformations in Ln_2O_3 through a defect-driven mechanism, where the generation of oxygen Frenkel pairs eventually produced ordering of vacancies and interstitials [30]. Vacancies were shown to occupy the (222) planes, while interstitials occupied tetrahedrally coordinated constitutional vacancy sites. At sufficient defect concentrations, this ordering can yield a reconstructive transformation to the B-type phase.

Here, *ab initio* molecular dynamics show that electronic excitation create oxygen Frenkel pairs in both Gd_2O_3 and Lu_2O_3. It should be noted that the purpose of these simulations was not to replicate the experimental conditions induced by 40-J/cm^2 irradiation. Rather, they were undertaken to under-
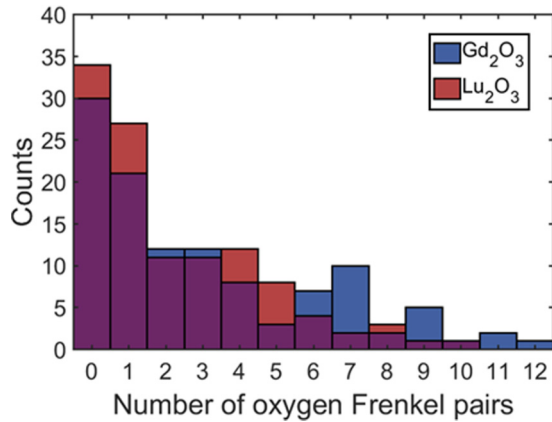
FIG. 4. Results from *ab initio* molecular dynamics showing the distribution of the number of oxygen Frenkel pairs produced in each simulation. Purple indicates overlap of the Gd_2O_3 (blue) and Lu_2O_3 (red) datasets. The results presented here define only a qualitative trend in the effect of changing the Ln cation due to approximations made in the simulations.

stand how electronic excitation alone can cause atomic motion due to the alteration of interatomic potentials and ultimately produce defects. No cation Frenkel pairs were observed in the simulations, consistent with their relatively high defect formation enthalpies [56]. The vast majority ($\sim$95%) of the oxygen interstitials in both compounds occupied tetrahedrally coordinated constitutional vacancies sites in the cubic structure, which is the first step in the C$\rightarrow$B transformation mechanism [30]. The remaining interstitials ($\sim$5%) occupied octahedral sites. The number of oxygen Frenkel pairs generated in each simulation are shown in Fig. 4. More oxygen Frenkel pairs were generated in Gd_2O_3 (average of 3.03 ± 0.35) than Lu_2O_3 (average of 2.20 ± 0.28). This is consistent with the denser atomic packing in Lu_2O_3 as compared with Gd_2O_3 [30].

We note that the band gap is underestimated relative to experimental values due to the use of the generalized gradient approximation in the current simulations. As a consequence, the number of defects formed is likely to be overestimated relative to what would be obtained at the same electronic temperature from simulations based on a higher level of theory where the band gap would be more accurately described.

However, our calculations demonstrate that oxygen Frenkel pairs can be produced, and that there is a trend of decreasing oxygen Frenkel pair population with increasing atomic packing in Ln_2O_3. These conclusions would not be changed by higher-level calculations.

IV. CONCLUSION

A C$\rightarrow$B phase transformation was induced in Ln_2O_3 (Ln = Er–Lu) by ultrafast laser irradiation at $40 \, J/cm^2$. GIXRD results indicated a markedly greater fraction of B-type phase in Er_2O_3 relative to the other compositions, suggesting that there may be a difference in transformation mechanism. Depth-dependent TEM analysis constrained the transformation mechanism based on the spatial separation of heat- and pressure-affected regions in the irradiated materials. The transformation in Lu_2O_3 was attributed to a pressure-driven process, in agreement with the known equilibrium high-pressure C$\rightarrow$B polymorphic transformation in heavy lanthanide sesquioxides. However, the transformation in Er_2O_3 was attributed to a thermally driven process, demonstrating that the nonequilibrium conditions of ultrafast laser irradiation can enable unexpected phase-transformation pathways. *Ab initio* molecular dynamics showed that electronic excitation generates oxygen Frenkel pairs, with the vast majority of interstitials migrating to tetrahedrally coordinated constitutional vacancy sites, the first step in a defect-driven C$\rightarrow$B transformation mechanism.

[1] B. Rethfeld, K. Sokolowski-Tinten, D. Von Der Linde, and S. I. Anisimov, Appl. Phys. A: Mater. Sci. Process. **79**, 767 (2004).

[2] S. K. Sundaram and E. Mazur, Nat. Mater. **1**, 217 (2002).

[3] D. Von der Linde, K. Sokolowski-Tinten, and J. Bialkowski, Appl. Surf. Sci. **109-110**, 1 (1997).

[4] M. J. Abere, C. Chen, D. R. Rittman, M. Kang, R. S. Goldman., J. D. Phillips, B. Torralva, and S. M. Yalisove, Appl. Phys. Lett. **105**, 163103 (2014).

[5] J. Bonse, J. Krüger, S. Höhm, and A. Rosenfeld, J. Laser Appl. **24**, 042006 (2012).

[6] Q. Feng, Y. N. Picard, H. Liu, S. M. Yalisove, G. Mourou, and T. M. Pollock, Scr. Mater. **53**, 511 (2005).

[7] Q. Feng, Y. N. Picard, J. P. McDonald, P. A. Van Rompay, S. M. Yalisove, and T. M. Pollock, Mater. Sci. Eng. A **430**, 203 (2006).

[8] D. R. Rittman, C. L. Tracy, A. B. Cusick, M. J. Abere, B. Torralva, R. C. Ewing, and S. M. Yalisove, Appl. Phys. Lett. **106**, 171914 (2015).

[9] F. Costache, S. Kouteva-Arguirova, and J. Reif, Appl. Phys. A, **79**, 1429 (2004).

[10] M. J. Smith, Y. T. Lin, M. J. Sher, M. T. Winkler, E. Mazur, and S. Gradečak, J. Appl. Phys. **110**, 053524 (2011).

[11] M. Tsujino, T. Sano, O. Sakata, N. Ozaki, and S. Kimura, J. Appl. Phys. **110**, 126103 (2011).

[12] L. Rapp, B. Haberl, C. J. Pickard, J. E. Bradby, E. G. Gamaly, J. S. Williams, and A. V. Rode, Nat. Commun. **6**, 7555 (2015).

[13] A. Vailionis, E. G. Gamaly, V. Mizeikis, W. Yang, A. V. Rode, and S. Juodkazis, Nat. Commun. **2**, 445 (2011).

[14] A. Rousse, C. Rischel, S. Fourmaux, I. Uschmann, S. Sebban, G. Grillon, P. Balcou, E. Förster, J. P. Geindre, P. Audebert, J. C. Gauthier, and D. Hulin, Nature (London) **410**, 65 (2001).

[15] A. M. Lindenberg, J. Larsson, K. Sokolowski-Tinten, K. J. Gaffney, C. Bolme, O. Synnergren, J. Sheppard, C. Caleman, A. G. MacPhee, D. Weinstein, and D. P. Lowney, Science **308**, 392 (2005).

[16] M. J. Abere, B. Torralva, and S. M. Yalisove, Appl. Phys. Lett. **108**, 153110 (2016).

[17] J. Courtures, A. Rouanet, R. Verges, and M. Foex, J. Solid State Chem. **17**, 171 (1976).

[18] Q. Guo, Y. Zhao, C. Jiang, W. L. Mao, Z. Wang, J. Zhang, and Y. Wang, Inorg. Chem. **46**, 6164 (2007).

[19] Q. Guo, Y. Zhao, C. Zhang, W. L. Mao, and Z. Wang, Solid State Commun. **145**, 250 (2008).

[20] S. Jiang, J. Liu, C. Lin, L. Bai, W. Xiao, Y. Zhang, D. Zhang, X. Li, Y. Li, and L. Tang, J. Appl. Phys. **108**, 083541 (2010).

[21] S. Jiang, J. Liu, X. Li, L. Bai, W. Xiao, Y. Zhang, C. Lin, Y. Li, and L. Tang, J. Appl. Phys. **110**, 013526 (2011).

[22] S. Jaing, J. Liu, C. Lin, L. Bai, Y. Zhang, X. Li, Y. Li, L. Thang, and H. Wang, Solid State Commun. **169**, 37 (2013).

[23] M. J. Lipp, J. R. Jeffries, H. Cynn, J. H. Park Klepeis, W. J. Evans, D. R. Mortensen, G. T. Seidler, Y. Xiao, and P. Chow, Phys. Rev. B **93**, 064106 (2016).

[24] J. P. McClure, Ph.D. thesis, University of Nevada Las Vegas, 2009.

[25] C. Meyer, J. P. Sanchez, J. Thomasson, and J. P. Itie, Phys. Rev. B **51**, 12187 (1995).

[26] K. K. Pandey, N. Garg, A. K. Mishra, and S. M. Sharma, J. Phys.: Conf. Ser. **377**, 012006 (2012).

[27] J. Sheng, B. Li-Gang, L. Jing, X. Wan-Sheng, L. Xiao-Dong, L. Yan-Chun, T. Ling-Yun, Z. Yu-Feng, Z. De-Chun, and Z. Li-Rong, Chin. Phys. Lett. **26**, 076101 (2009).

[28] F. X. Zhang, M. Lang, J. W. Wang, U. Becker, and R. C. Ewing, Phys. Rev. B **78**, 064114 (2008).

[29] G. Chen and J. R. Peterson, J. Alloys Compd. **186**, 233 (1992).

[30] C. L. Tracy, M. Lang, F. Zhang, C. Trautmann, and R. C. Ewing, Phys. Rev. B **92**, 174101 (2015).

[31] C. Prescher, V. B. Prakapenka, High Press. Res. **35**, 223 (2015).

[32] L. Lutterotti, S. Matthies, and H. R. Wenk, IUCr Newsl. CPD **21**, 14 (1999).

[33] J. S. Graves and R. E. Allen, Phys. Rev. B **58**, 13627 (1998).

[34] V. Recoules, J. Clerouin, G. Zerah, P. M. Anglade, and S. Mazevet, Phys. Rev. Lett. **96**, 055503 (2006).

[35] P. L. Silvestrelli, A. Alavi, M. Parrinello, and D. Frenkel, Phys. Rev. Lett. **77**, 3149 (1996).

[36] P. Stampfli and K. H. Bennemann, Phys. Rev. B **42**, 7163 (1990).

[37] P. Stampfli and K. H. Bennemann, Phys. Rev. B **46**, 10686 (1992).

[38] P. Stampfli and K. H. Bennemann, Phys. Rev. B **49**, 7299 (1994).

[39] E. S. Zijlstra, A. Kalitsov, T. Zier, and M. E. Garcia, Adv. Mater. **25**, 5605 (2013).

[40] E. S. Zijlstra, J. Walkenhorst, and M. E. Garcia, Phys. Rev. Lett. **101**, 135701 (2008).

[41] J. P. Perdew, K. Burke, and M. Ernzerhof, Phys. Rev. Lett. **77**, 3865 (1996).

[42] P. E. Blöchl, Phys. Rev. B **50**, 17953 (1994).

[43] G. Kresse and D. Joubert, Phys. Rev. B **59**, 1758 (1999).

[44] G. Kresse and J. Furthmüller, Phys. Rev. B **54**, 11169 (1996).

[45] G. Kresse and J. Hafner, Phys. Rev. B **47**, 558(R) (1993).

[46] H. Jiang, P. Rinke, and M. Scheffler, Phys. Rev. B **86**, 125115 (2012).

[47] See Supplemental Material at http://link.aps.org/supplemental/10.1103/PhysRevB.97.024104 for additional *ab initio* simulation details.

[48] J. P. Colombier, P. Combis, F. Bonneau, R. Le Harzic, and E. Audouard, Phys. Rev. B **71**, 165406 (2005)

[49] R. Evans, A. D. Badger, F. Fallies, M. Mahdieh, T. A. Hall, P. Audebert, J. P. Geindre, J. C. Gauthier, A. Mysyrowicz, G. Grillon, and A. Antonetti, Phys. Rev. Lett. **77**, 3359 (1996).

[50] L. Huang, Y. Yang, Y. Wang, Z. Zheng, and W. Su, J. Phys. D: Appl. Phys. **42**, 045502 (2009).

[51] M. E. Povarnitsyn, T. E. Itina, K. V. Khishchenko, and P. R. Levashov, Appl. Surf. Sci. **253**, 6343 (2007).

[52] T. H. R. Crawford, J. Yamanaka, G. A. Botton, and H. K. Haugen, J. Appl. Phys. **103**, 053104 (2008).

[53] R. Le Harzic, N. Huot, E. Audouard, C. Jonin, P. Laporte, S. Valette, A. Fraczkiewicz, and R. Fortunier, Appl. Phys. Lett. **80**, 3886 (2002).

[54] M. Tsujino, T. Sano, T. Ogura, M. Okoshi, N. Inoue, N. Ozaki, R. Kodama, K. F. Kobayashi, and A. Hirosi, Appl. Phys. Express **5**, 022703 (2012).

[55] G. Baldinozzi, D. Simeone, D. Gosset, I. Monnet, S. Le Caër, and L. Mazerolles, Phys. Rev. B **74**, 132107 (2006).

[56] A. Chroneos, M. R. Levy, C. R. Stanek, K. McClellan, and R. W. Grimes, Phys. Stat. Sol. C **4**, 1213 (2007).